

Jones-matrix dual-comb spectroscopic polarimetry

Hidenori Koresawa^{1,†}, Hiroki Kitahama², Eiji Hase³, Yu Tokizane³, Akifumi Asahara⁴,
Takeo Minamikawa³, Kaoru Minoshima⁴, and Takeshi Yasui¹

¹Graduate School of Advanced Technology and Science, Tokushima University, 2-1
Minami-Josanjima, Tokushima, Tokushima 770-8506, Japan

²Graduate School of Sciences and Technology for Innovation, Tokushima University,
2-1, Minami-Josanjima, Tokushima 770-8506, Japan

³Institute of Post-LED Photonics (pLED), Tokushima University, 2-1, Minami-
Josanjima, Tokushima 770-8506, Japan

⁴Graduate School of Informatics and Engineering, The University of Electro-
Communications, 1-5-1 Chofugaoka, Chofu, Tokyo 182-8585, Japan

Abstract

Spectroscopic polarimetry (SP) is a powerful tool for evaluation of thin film, optical materials, and biological samples because it can provide both polarimetric and spectroscopic characteristics of objects. However, its performance is often hampered by the mechanical instability and the limited data acquisition speed arising from the mechanical polarization modulation. Dual-comb spectroscopic polarimetry (DCSP) based on a combination of SP with dual-comb spectroscopy can acquire optical spectra of amplitude ratio and phase difference in p- and s-polarization components of the output light from simultaneous measurement of optical spectra of optical amplitude and phase in p- and s-polarization components without the need for mechanical polarization modulation. In this article, we combine the DCSP with polarization control pulse sequences (PCPS) with different polarizations and time delays for a more detailed analysis of the sample's polarization response based on Jones matrix. We obtain Jones matrix of a sample as a function of wavelength by measuring those optical spectra while multiplexing the incident light into multiple polarizations instead of a single polarization. Such Jones matrix DCSP (JM-DCSP) is applied for analysis of optical elements with known polarization property and its experimental result is in good agreement with theoretical values, indicating the validity of the proposed method. JM-DCSP will further expand the application scope of SP.

1. Introduction

Spectroscopic polarimetry (SP) or spectroscopic ellipsometry [1] is a technique that combines spectroscopy and polarimetry to analyze the polarization properties of light as a function of its wavelength or optical frequency. Measuring the polarization state of light at different wavelengths enables us to obtain valuable information about the interaction of light with matter such as optical activity, birefringence, and circular dichroism. Therefore, SP has applications in diverse areas, including the evaluation of refractive index and thickness of thin film [2], the characterization of optical materials [3], and the investigation of biological samples [4]. In usual SPs, an optical spectrum is measured while modulating the polarization of the incident or the output light, mechanically [5]. However, such mechanical polarization modulation limits the mechanical stability and the data acquisition time (typically, several tens of milliseconds) of the SP system.

Recently, optical frequency comb (OFC) has attracted attention as a light source for polarization-modulation-free SP [6-9]. OFC [10-12] can be perceived as an ensemble of tens of thousands of individually phase-locked single-wavelength lasers with equal frequency intervals ($= f_{rep}$), combining a broadband spectral characteristic with narrow linewidth mode properties. Also, dual-comb spectroscopy (DCS) [13-16] enables rapid, precise acquisition of mode-resolved OFC spectra of optical amplitude and phase by interfering two OFCs with slightly different f_{rep} to generate a secondary frequency comb of optical beat signals in RF region (namely, RF comb). In dual-comb spectroscopic polarimetry (DCSP) based on a combination of SP with DCS [5-8], optical spectra of amplitude ratio ψ and phase difference Δ can be obtained without polarization modulation by acquiring mode-resolved OFC spectra of optical amplitude

and phase in p- and s-polarization component of the output light. The resulting polarization-modulation-free characteristic in DCSP does not suffer from the instability of polarization modulation and improve the performance of SP. Effectiveness of DCSP was demonstrated by applying it for analysis of a thin film [6,8] and a time-resolved polarization measurement of a dynamic sample [7,8].

In the previous studies of DCSP, the polarization analysis of the output light from the sample in response to incident light with a single polarization was performed. If the incident light is multiplexed into multiple polarizations instead of a single polarization, it would enable a more detailed analysis of the sample's polarization response. In other words, use of multiple polarizations in the incident light can further advance the performance of DCSP. For example, if two different polarizations are used for the incident light of DCSP, Jones matrix of a sample can be acquired as a function of wavelength. The Jones matrix is a 2x2 matrix that relates the input polarization state of light to the output polarization state after passing through an optical element or system; it is often used to describe the polarization state of light as it propagates through an optical element or system. The elements of the matrix represent the complex amplitudes of the electric field components parallel and perpendicular to a reference axis. To obtain the Jones matrix, polarization analysis of the output light for two different incident polarizations is required.

In this article, we developed Jones matrix DCSP (JM-DCSP). Polarization control pulse sequences (PCPS) with different polarizations and time delays are generated by separating a single optical pulse of OFC into different optical paths and then adding different time delay and the polarization control on each of them. The DCSP of PCPS enables Jones matrix SP without the need for polarization modulation,

benefiting from the rapid, precise, data acquisition. We measured polarization elements with known polarization property to demonstrate the effectiveness of JM-DCSP.

2. Principle of operation

2.1 Jones calculus

The polarization state of light is determined by the relative amplitudes and phases of the orthogonal x-polarized component E_x and y-polarized component E_y in electric field. This polarization state is represented using the Jones vector \mathbf{J} , expressed by

$$\mathbf{J} = \begin{bmatrix} E_x \\ E_y \end{bmatrix} = \begin{bmatrix} E_{x0} \cdot e^{i\phi_x} \\ E_{y0} \cdot e^{i\phi_y} \end{bmatrix}, \quad (1)$$

where E_{x0} and E_{y0} respectively represent the amplitudes of the x-polarized component and y-polarized component whereas ϕ_x and ϕ_y represent the phases of the x-polarized component and y-polarized component, respectively. By normalization, Eq. (1) can be simplified as follows:

$$\mathbf{J} = \begin{bmatrix} E_{x0} \cdot e^{i\phi_x} \\ E_{y0} \cdot e^{i\phi_y} \end{bmatrix} \Rightarrow \begin{bmatrix} \sin\psi \cdot e^{i\Delta} \\ \cos\psi \end{bmatrix}, \quad (2)$$

where ψ and Δ represent the amplitude ratio and phase difference, respectively, between the x-polarized component and y-polarized component.

Next, polarization property of optical elements is represented using the Jones matrix M by

$$M = \begin{bmatrix} J_{00} & J_{01} \\ J_{10} & J_{11} \end{bmatrix} \quad (3)$$

where J_{00} , J_{01} , J_{10} , and J_{11} are the complex elements of the Jones matrix. For example, the Jones matrices for birefringent material (M_b) and optically active material (M_a),

respectively, are represented by

$$M_b = \begin{bmatrix} 1 & 0 \\ 0 & e^{ib} \end{bmatrix} \quad (4)$$

$$M_r = \begin{bmatrix} \cos r & -\sin r \\ \sin r & \cos r \end{bmatrix} \quad (5)$$

where b and r represent the phase differences due to birefringence and the optical rotation angle, respectively. The Jones matrix for birefringent material with the polarization axis rotated by an angle θ from the x-axis [$M_b(\theta)$] is represented by

$$M_b(\theta) = \begin{bmatrix} \cos\theta & -\sin\theta \\ \sin\theta & \cos\theta \end{bmatrix} \cdot M_b \cdot \begin{bmatrix} \cos\theta & \sin\theta \\ -\sin\theta & \cos\theta \end{bmatrix} \quad (6)$$

After passing through a polarization optical element given by M , the polarization state of incident light given by \mathbf{J} is transformed to a polarization state of output light given by \mathbf{J}' . This transformation can be expressed using the Jones calculus as follows:

$$\mathbf{J}' = M \cdot \mathbf{J} \quad (7)$$

2.2 Generation of polarization control pulse sequences

Figure 1 illustrates a schematic drawing of experimental setup to generate PCPS. In this article, we define x- and y-polarization to be horizontal (or 0°) polarization and vertical (or $+90^\circ$) polarization, respectively. A single OFC pulse with x-polarization is initially split into transmitted and reflected OFC pulses by a beam splitter (BS). The transmitted OFC pulse is used for generation the first polarization-controlled pulse (PCP, see orange line) whereas the reflected OFC pulse is used for generation the second PCP (see green line). The transmitted OFC pulse maintains x-polarization. The polarization and time delay of the reflected OFC pulse are controlled to be y-polarization and a time delay of $\Delta\tau$ from the first PCP in order to have the different polarization and time delay of the first PCP. Then, those two OFC pulses are recombined by a polarization beam splitter (PBS) and pass through a half-wave plate ($\lambda/2$) to rotate their polarization by $+45^\circ$. In this way, PCPS composed of the first PCP

(+45° linear polarization, time delay = 0) and the second PCP (+135° linear polarization, time delay = $\Delta\tau$) are generated.

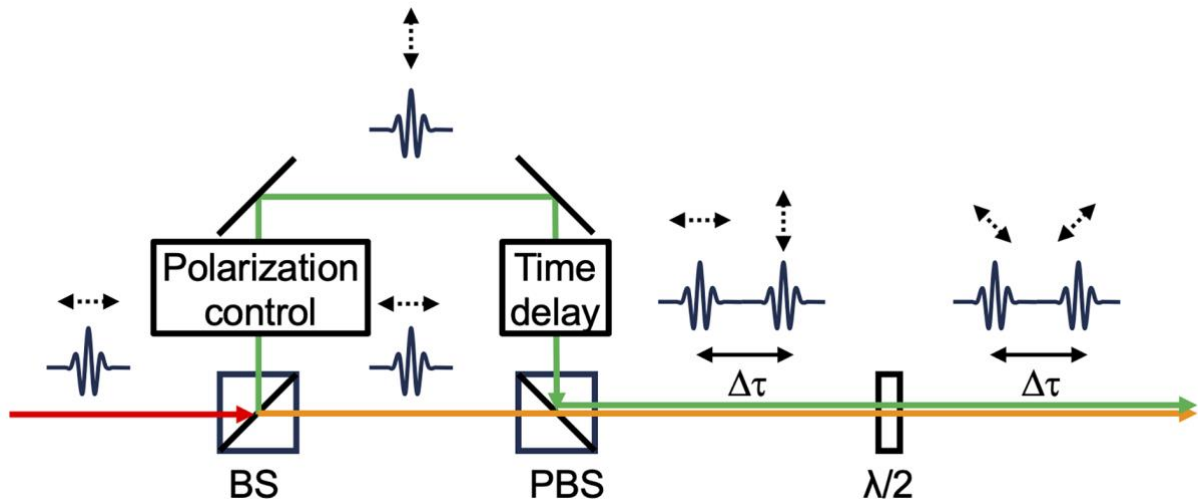


Fig. 1. Experimental setup for generation of PCPS. BS, beam splitter; PBS, polarization beam splitter; $\lambda/2$, a half-wave plate.

2.3 Dual-comb spectroscopy of polarization control pulse sequences

Figure 2 illustrates a schematic drawing of experimental setup for DCSP of PCSP. The PCPS described above passes through the sample, and each pulse undergoes changes in polarization condition reflecting the sample's optical properties. Subsequently, the PCPS interfere with a local OFC at a beam splitter (BS) for DCS. The generated interferogram was split into x-polarized and y-polarized components using a polarization beam splitter (PBS), and was detected by a pair of photodetectors (PDs). Subsequently, by performing Fourier transform of the acquired interferogram, the optical amplitude spectra and optical phase spectra of the first PCP and the second PCP are obtained with respect to x-polarized and y-polarized components. These spectra are then utilized in the Jones calculus to obtain the Jones matrix of the sample.

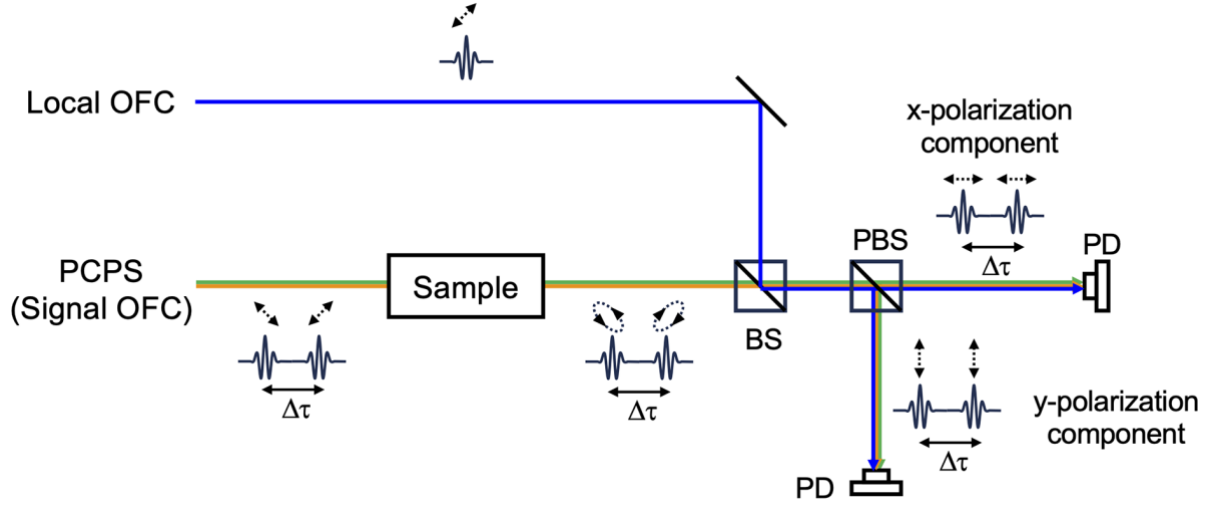


Fig. 2. DCS of PCPS. BS, beam splitter; PBS, polarization beam splitter; PD, photodiode.

Next, we describe the method for deriving the Jones matrix using JM-DCSP.

First, the polarization states of the two incident polarized pulses before passing through the sample are represented by the Jones vectors, \mathbf{J}_1 and \mathbf{J}_2 , given by

$$\mathbf{J}_1 = \begin{bmatrix} \sin\psi_1 \cdot e^{i\Delta_1} \\ \cos\psi_1 \end{bmatrix}, \quad (8)$$

$$\mathbf{J}_2 = \begin{bmatrix} \sin\psi_2 \cdot e^{i\Delta_2} \\ \cos\psi_2 \end{bmatrix}, \quad (9)$$

where ψ_1 and Δ_1 respectively represent the amplitude ratio and phase difference between the x-polarized and y-polarized components of the first PCP; similarly, ψ_2 and Δ_2 respectively represent the amplitude ratio and phase difference between the x-polarized and y-polarized components of the second PCP. Conversely, the polarization states of the two PCPs after passing through the sample are represented by the Jones vectors \mathbf{J}'_1 and \mathbf{J}'_2 , as follows

$$\mathbf{J}'_1 = \begin{bmatrix} E_{x1} \cdot e^{i\phi_{x1}} \\ E_{y1} \cdot e^{i\phi_{y1}} \end{bmatrix}, \quad (10)$$

$$\mathbf{J}'_2 = \begin{bmatrix} E_{x2} \cdot e^{i\phi_{x2}} \\ E_{y2} \cdot e^{i\phi_{y2}} \end{bmatrix}. \quad (11)$$

where E_{x1} and E_{y1} respectively represent the amplitudes of the x-polarized and y-polarized components of the first PCP, while Φ_{x1} and Φ_{y1} represent their respective phases. Similarly, E_{x2} and E_{y2} respectively represent the amplitudes of the x-polarized and y-polarized components of the second PCP, while Φ_{x2} and Φ_{y2} represent their respective phases. By substituting Eqs. (3), (7), (8), and (9), Eqs. (10) and (11) are given by

$$J'_1 = \begin{bmatrix} E_{x1} \cdot e^{i\Phi_{x1}} \\ E_{y1} \cdot e^{i\Phi_{y1}} \end{bmatrix} = \begin{bmatrix} J_{00} & J_{01} \\ J_{10} & J_{11} \end{bmatrix} \cdot \begin{bmatrix} \sin\psi_1 \cdot e^{i\Delta_1} \\ \cos\psi_1 \end{bmatrix}, \quad (12)$$

$$J'_2 = \begin{bmatrix} E_{x2} \cdot e^{i\Phi_{x2}} \\ E_{y2} \cdot e^{i\Phi_{y2}} \end{bmatrix} = \begin{bmatrix} J_{00} & J_{01} \\ J_{10} & J_{11} \end{bmatrix} \cdot \begin{bmatrix} \sin\psi_2 \cdot e^{i\Delta_2} \\ \cos\psi_2 \end{bmatrix}. \quad (13)$$

Ultimately, the elements of the Jones matrix can be derived by

$$\begin{bmatrix} J_{00} \\ J_{01} \end{bmatrix} = \begin{bmatrix} \sin\psi_1 \cdot e^{i\Delta_1} & \cos\psi_1 \\ \sin\psi_2 \cdot e^{i\Delta_2} & \cos\psi_2 \end{bmatrix}^{-1} \cdot \begin{bmatrix} E_{x1} \cdot e^{i\Phi_{x1}} \\ E_{x2} \cdot e^{i\Phi_{x2}} \end{bmatrix} \quad (14)$$

$$\begin{bmatrix} J_{10} \\ J_{11} \end{bmatrix} = \begin{bmatrix} \sin\psi_1 \cdot e^{i\Delta_1} & \cos\psi_1 \\ \sin\psi_2 \cdot e^{i\Delta_2} & \cos\psi_2 \end{bmatrix}^{-1} \cdot \begin{bmatrix} E_{y1} \cdot e^{i\Phi_{y1}} \\ E_{y2} \cdot e^{i\Phi_{y2}} \end{bmatrix} \quad (15)$$

3. Experimental setup

Based on the concept described above, we constructed an experimental setup of JM-DCSP as shown in Fig. 3. As a partial revision, in order to determine the absolute phase of the 1st PCP and the 2nd PCP, an additional reference pulse is generated. This reference pulse is also multiplexed with PCPS to achieve a certain time delay from the second PCP, resulting in the generation of three distinct pulse sequences, each possessing its unique polarization.

A pair of mode-locked erbium-doped fiber OFCs (Neoark Co., Japan, OCLS-HSC-D100-TKSM, center wavelength = 1562 nm, spectral bandwidth = 50 nm) was used for a signal OFC ($f_{rep1} = 100$ MHz, $f_{ceo1} = 10.5$ MHz) and a local OFC ($f_{rep2} =$

99.99968 MHz, $f_{ceo2} = 10.5$ MHz; $\Delta f_{rep} = f_{rep1} - f_{rep2} = 320$ Hz) in JM-DCSP. These OFCs are phase-locked to a rubidium frequency standard (Rb-Fs, Stanford Research Systems, Inc., FS725, frequency = 10 MHz, accuracy = 5×10^{-11} , instability = 2×10^{-11} at 1 s), and the local OFC was tightly and coherently locked to the signal OFC with a constant Δf_{rep} using a narrow-linewidth continuous-wave (CW) laser (CWL1) for intermediate laser (not shown in Fig. 3). This enables coherent averaging of the interferogram between the signal and local OFCs.

An optical pulse of a signal OFC (OFC pulse) was split into a transmitted OFC pulse for PCPS (x-polarization, see red line) and a reflected OFC pulse for a reference pulse (y-polarization, see purple line) after adjusting their power split ratio of 1:2 by a combination of a quarter-wave plate ($\lambda/4$), a half-wave plate ($\lambda/2$), and a polarization beam splitter (PBS). The transmitted OFC pulse was further split into the first PCP (see orange line) and the second PCP (see green line) by a beam splitter (BS). The polarization of the first and the second PCPs was adjusted to be x-polarization and y-polarization while maintaining the similar optical power by a pair of $\lambda/2$ and a PBS. Difference between their optical pathlengths causes a time delay of 0.63 ns between the first and second PCPs. Then, the first PCP and the second PCP were spatially overlapped again by PBS, resulting in generation of PCPS. As the following $\lambda/2$ rotates the polarization of PCPS by $+45^\circ$, the polarization before a sample was set to be $+45^\circ$ for the first PCP and $+135^\circ$ for the second PCP. The PCPS undergoes the optical property of a sample, and its polarization changes. The reference pulse passed through a polarizer (P, polarization angle = $+45^\circ$) and then was combined with the PCPS by BS. This reference pulse has $+45^\circ$ linear polarization and was time-delayed by 0.15 ns from the second PCP. A pulse train triple consisting of the first PCP, the

second PCP, and the reference pulse was fed into the optical setup for DCSP. The optical systems for the first PCP, the second PCP, and the reference pulse were enclosed in a plastic box to suppress the influence of environmental disturbances such as atmospheric turbulence.

The local OFC has $+45^\circ$ linear polarization after passing through $\lambda/4$, $\lambda/2$, and P; then, it was spatially overlapped with the combined PCPS and reference pulse by BS to generate the interferogram. An optical bandpass filter (BPF, center wavelength = 1560 ± 2 nm, FWHM = 12 ± 2.4 nm) was used to suppress the aliasing effect in the acquisition of the interferogram. The x- and y-polarization components of the interferogram were respectively detected by a combination of PBS and a pair of photodiodes (PDs), and then acquired by a digitizer (not shown). The acquired signal is an interferogram sequence composed of the first PCP, the second PCP, and the reference pulse. For each 1st PCP, 2nd PCP, and reference pulse, only the interferogram signal is temporally extracted, and zero padding is applied to the remaining data outside of the extracted portion. This process allows separating the 1st PCP, 2nd PCP, and reference pulse to obtain their respective interferograms with a time window size of $1/f_{rep1}$. Then, they were respectively Fourier-transformed to obtain the mode-resolved OFC spectra of amplitude and phase in the x- and y-polarization components. The amplitude and phase spectra of the first and the second PCPs were used to obtain Δ and ψ spectra of a sample whereas the phase difference spectra between the first PCP (or the second PCP) and the reference pulse were used to calculate the absolute phase spectra of the first PCP (or the second PCP).

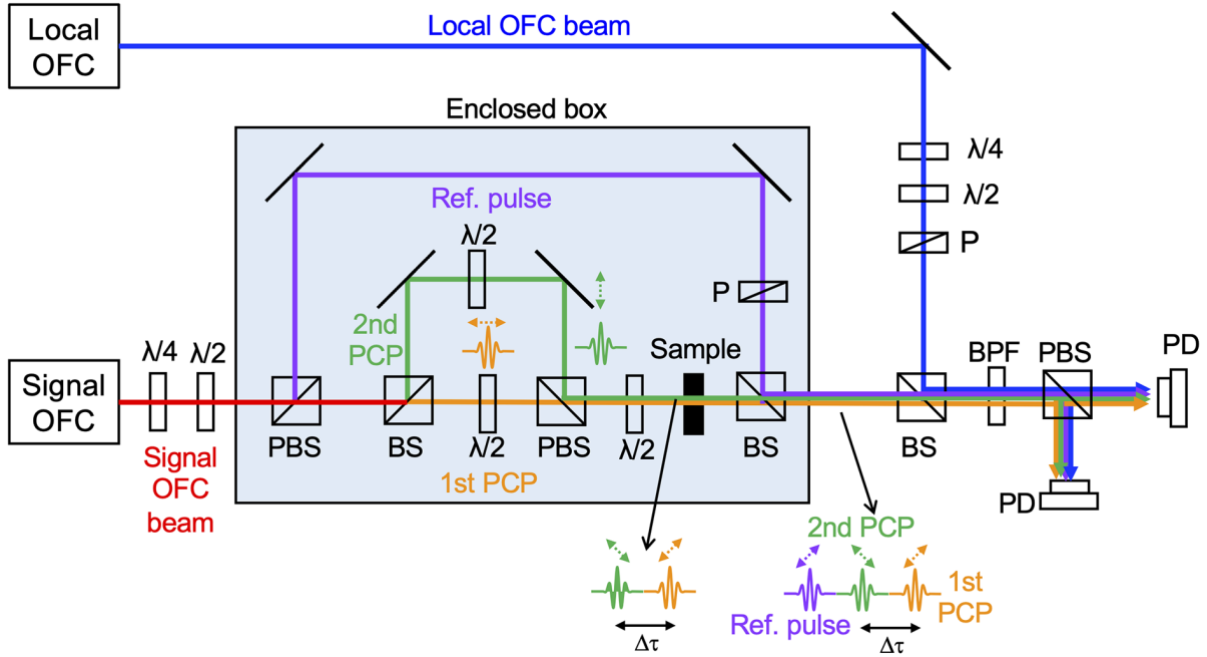


Fig. 3. Experimental setup of JM-DCSP. $\lambda/4$, quarter-wave plate; $\lambda/2$, a half-wave plate; PBSs, polarization beam splitters; BSs, beam splitters; P, polarizer; BPF, optical bandpass filter; PDs, photodiodes.

4. Results

We first evaluated the basic performance of PCPS. Red and blue plots of Fig. 4(a) show interferograms of no samples with respect to x- and y-polarization components. The first PCP, the second PCP, and the reference pulse were observed with a time delay of 0.63 ns and 0.15 ns, respectively. In order to verify the validity of their configured polarizations, we next placed a polarizer at the sample position. The red and blue plots in Fig. 4(b) represent the x- and y-polarization components of the interferogram when the placed polarizer was oriented with its transmission axis set at $+45^\circ$. The first PCP and the reference pulse appeared whereas the second PCP disappeared as expected. Conversely, when the placed polarizer was oriented with its transmission axis set at $+135^\circ$, the second PCP and the reference pulse appeared

whereas the first PCP disappeared, as shown in Fig. 4(c). In this way, we verified the validity of the polarization for the first PCP, the second PCP, and the reference pulse.

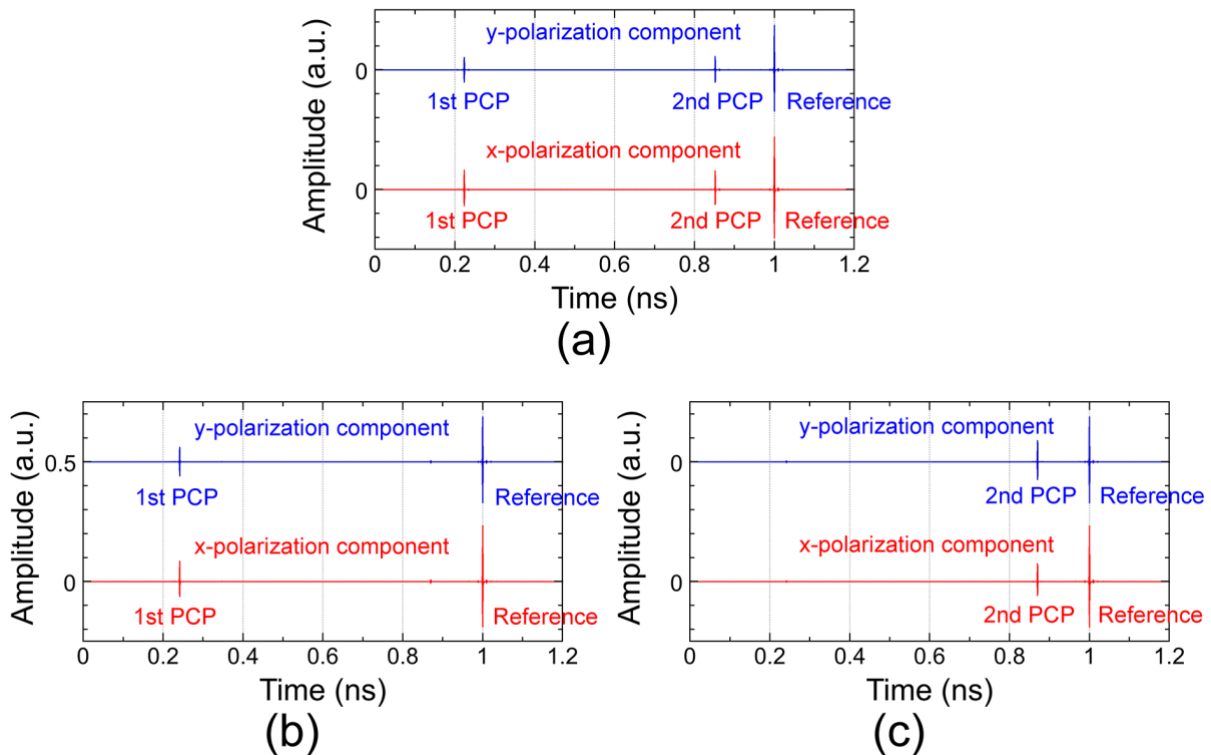


Fig. 4. (a) Interferogram of no samples with respect to x-polarization and y-polarization components. Interferogram with respect to x-polarization and y-polarization components when a transmission axis of the polarizer was orientated at an angle of (b) $+45^\circ$ and (c) $+135^\circ$.

We next measured polarization elements with known polarization property to demonstrate the effectiveness of JM-DCSP. We used a zero-order quarter-wave plate (Thorlabs, WPQ05M-1550, wavelength = 1550 nm, retardance accuracy $< \lambda/300$) as the first sample with a known birefringence. Black plot of Fig. 5(a) shows a series of optical spectra of each Jones matrix component in the quarter-wave plate when its fast axis was set to be parallel to the y-polarization: (a-1) real part and (a-2) imaginary part of J_{00} (J_{00r} and J_{00i}), (a-3) real part and (a-4) imaginary part of J_{01} (J_{01r} and J_{01i}),

(a-5) real part and (a-6) imaginary part of J_{10} (J_{10r} and J_{10i}), and (a-7) real part and (a-8) imaginary part of J_{11} (J_{11r} and J_{11i}), respectively (number of signal integration = 10,000). Only J_{00r} and J_{11i} are non-zero values whereas the others were zero. This result well reflects the Jones matrix M_b of the birefringent materials given by Eq. (4). For comparison, red plot of Fig. 5(a) shows the corresponding theoretical spectra of each Jones matrix component. The comparison between them indicated that the experimental result was in good agreement with the theoretical value for each Jones matrix component.

Each component of Jones matrix in the quarter-wave plate depends on the angle of the fast axis in addition to the birefringence, as shown by Eq. (6). To confirm such the angle dependence of Jones matrix component, the fast axis of the quarter-wave plate was rotated by $+40^\circ$ in a counterclockwise direction from the orientation along the y-axis, corresponding to an angle of $+130^\circ$. Black plot of Fig. 5(b) shows a series of optical spectra in each Jones matrix component: (b-1) J_{00r} , (b-2) J_{00i} , (b-3) J_{01r} , (b-4) J_{01i} , (b-5) J_{10r} , (b-6) J_{10i} , (b-7) J_{11r} , and (b-8) J_{11i} . Those spectra were different from that in Fig. 5(a) due to the angle dependence. For comparison, red plot of Fig. 5(b) shows the corresponding theoretical spectra of each Jones matrix component. The experimental result was in moderate agreement with the theoretical value for each Jones matrix component, again.

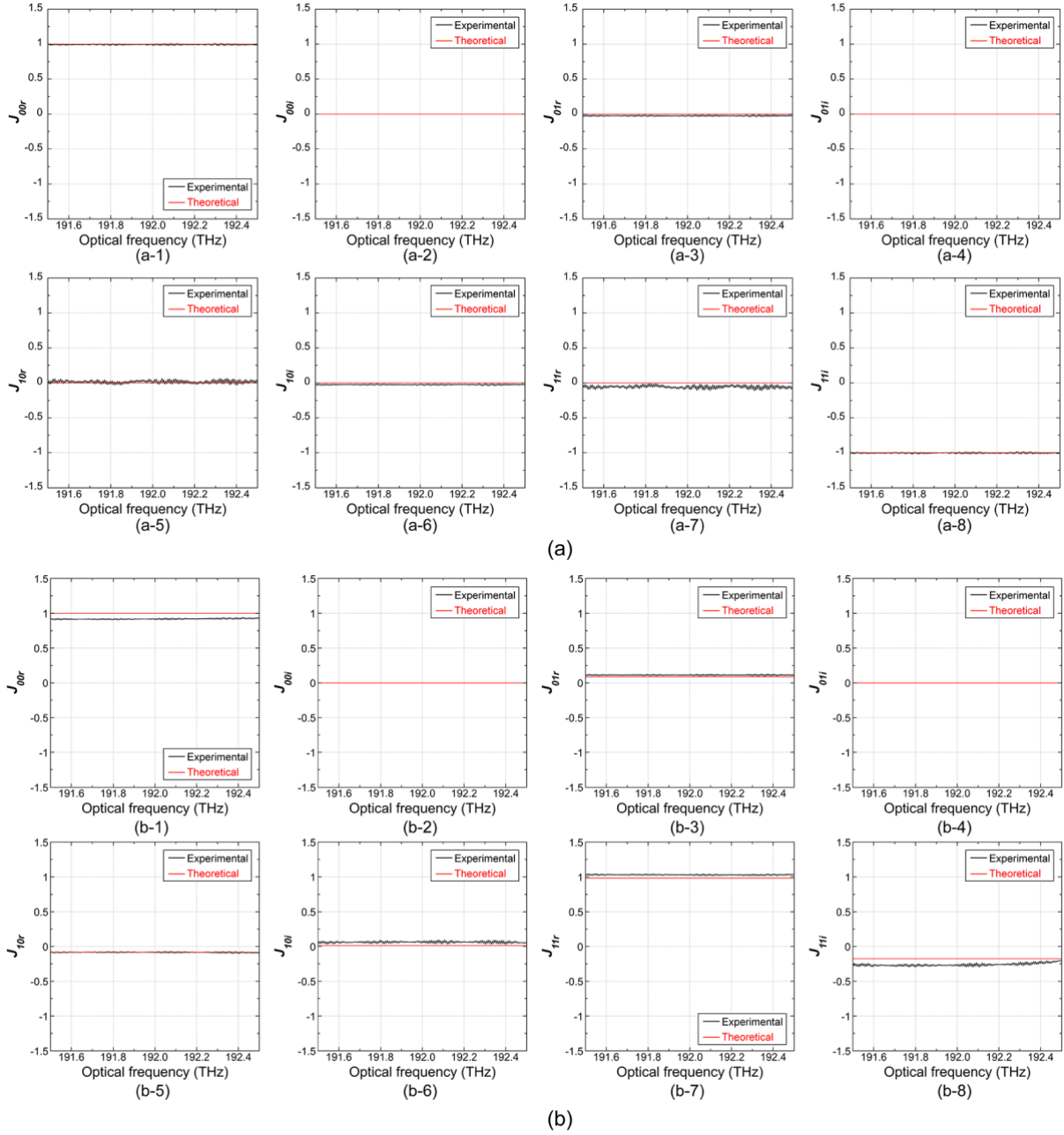


Fig. 5. Optical spectra of eight Jones matrix components in a zero-order quarter-wave plate (a) when its fast axis is parallel to the y-polarization. (a-1) J_{00r} , (a-2) J_{00i} , (a-3) J_{01r} , (a-4) J_{01i} , (a-5) J_{10r} , (a-6) J_{10i} , (a-7) J_{11r} , and (a-8) J_{11i} . Optical spectra of eight Jones matrix components in a zero-order quarter-wave plate (b) when its fast axis is orientated at an angle of $+150^\circ$. (b-1) J_{00r} , (b-2) J_{00i} , (b-3) J_{01r} , (b-4) J_{01i} , (b-5) J_{10r} , (b-6) J_{10i} , (b-7) J_{11r} , and (b-8) J_{11i} .

We also measured a multi-order quarter-wave plate (Thorlabs, WPMQ05M-1550, wavelength = 1550 nm, retardance accuracy $< \lambda/300$) when its fast axis was set to be parallel to the y-polarization. Black plot of Fig. 6 shows a series of optical spectra in each Jones matrix component: (a) J_{00r} , (b) J_{00i} , (c) J_{01r} , (d) J_{01i} , (e) J_{10r} , (f) J_{10i} , (g) J_{11r} , and (h) J_{11i} . Although the spectral bandwidth was limited by BPF, we confirmed the wavelength dependence in J_{11r} and J_{11i} .

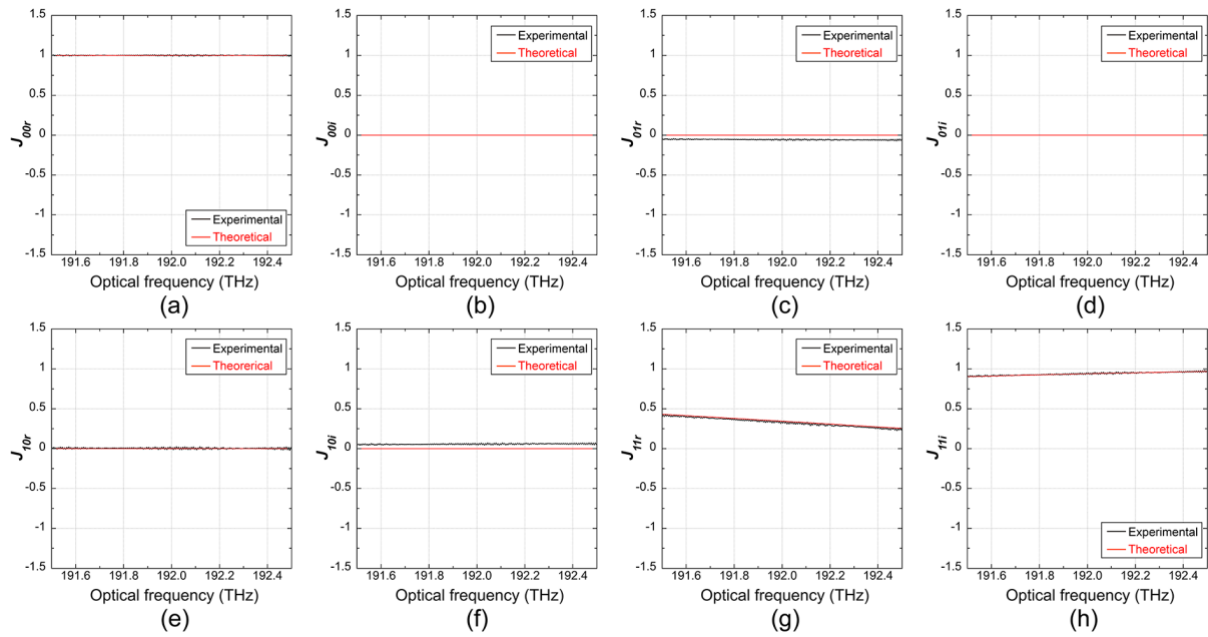


Fig. 6. Optical spectra of eight Jones matrix components in multi-order quarter-wave plate when its fast axis was parallel to the y-polarization. (a) J_{00r} , (b) J_{00i} , (c) J_{01r} , (d) J_{01i} , (e) J_{10r} , (f) J_{10i} , (g) J_{11r} , and (h) J_{11i} .

We also measured Jones matrix of a Faraday rotator (Thorlabs, I1550R5, rotation angle = $45 \pm 3^\circ$, minimum transmission = 98%, wavelength = 1500-1600 nm) as a sample of optically active material. When the first PCP with $+45^\circ$ linear polarization and the 2nd PCP with $+135^\circ$ linear polarization were used for the incident light of JM-DCSP, the first and second PCPs after passing through the Faraday rotator

have the y-polarization and x-polarization. This situation is corresponding to the dead zone of DCSP. To avoid it, we changed the polarization angle of the first PCP and the second PCP to be $+32^\circ$ and $+122^\circ$, respectively. Figure 7 compares the experimental data (black plot) with the theoretical value (red plot) regarding a series of optical spectra in each Jones matrix component: (a) J_{00r} , (b) J_{00i} , (c) J_{01r} , (d) J_{01i} , (e) J_{10r} , (f) J_{10i} , (g) J_{11r} , and (h) J_{11i} . A unique Jones matrix that is different from the quarter-wave plates (see Figs. 5 and 6) can be confirmed. The experimental data and the theoretical value were in good agreement with each other, again. Furthermore, when the Faraday rotator was rotated by $+60^\circ$, the optical spectra of each Jones matrix component did not change because of no angle dependence of optical rotation (not shown).

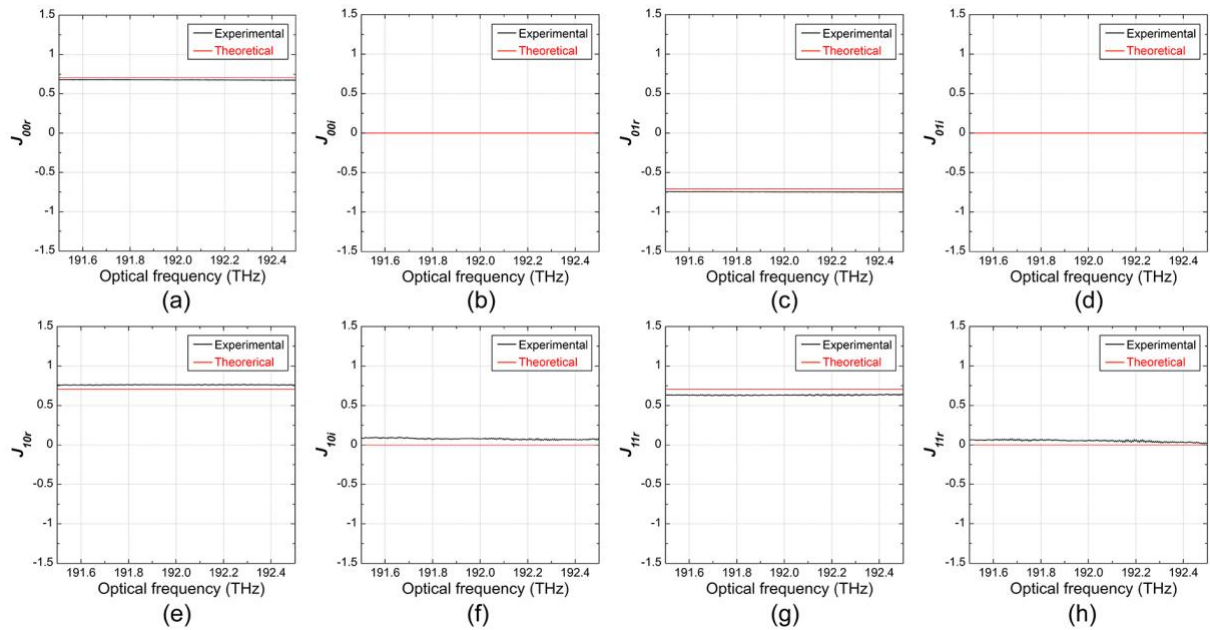


Fig. 7. Optical spectra of eight Jones matrix components in a Faraday rotator. (a) J_{00r} , (b) J_{00i} , (c) J_{01r} , (d) J_{01i} , (e) J_{10r} , (f) J_{10i} , (g) J_{11r} , and (h) J_{11i} .

Finally, we measured the combined Jones matrix for the series configuration of a Faraday rotator and a zero-order quarter-wave plate. In this case, the combined

Jones matrix can be expressed as the product of the Jones matrix of the Faraday rotator and the that of the quarter-wave plate. We here set the fast axis of the quarter-wave plate was to be an angle of $+130^\circ$. Black plot of Fig. 8 shows a series of measured optical spectra in each component of the combined Jones matrix: (a) J_{00r} , (b) J_{00i} , (c) J_{01r} , (d) J_{01i} , (e) J_{10r} , (f) J_{10i} , (g) J_{11r} , and (h) J_{11i} . These spectra well reflect the product of Jones matrices spectra in Figs. 5(b) and 7. Compared with their theoretical values as shown by red plot in Fig. 8, we confirmed the validity of the proposed method to the combined Jones matrix.

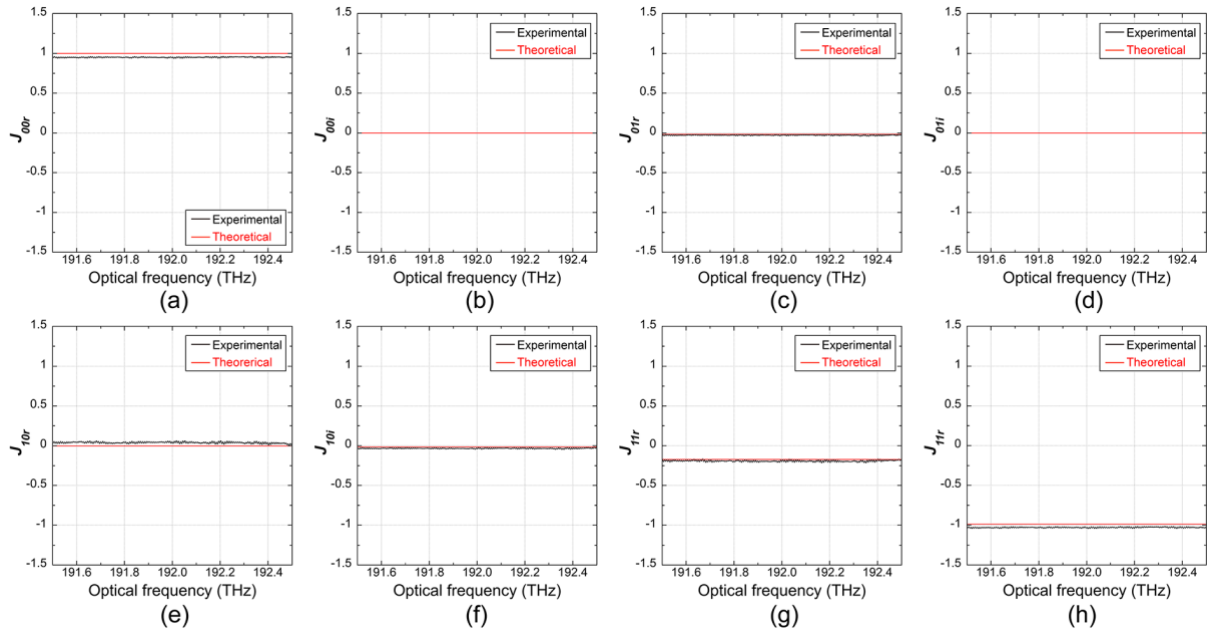


Fig. 8. Optical spectra of the combined Jones matrix in a Faraday rotator and a zero-order quarter-wave plate orientated at 130° .

5. Discussion

The experimental results measured by the JM-DCSP showed good agreement with the theoretical values, but some discrepancies were also observed. Here, we discuss the factors contributing to these discrepancies. One of the factors causing

errors is the fluctuation in the absolute phase due to environmental disturbances, including air turbulence. In the present setup, the absolute phase of the first PCP and second PCP is calculated by comparing them with the reference pulse. However, each optical path contains independent portions, leading to varying influences from environmental disturbances for each path. We attempted to enclose these optical systems in a plastic box to passively suppress the influence of environmental disturbances, but fluctuations in the absolute phase still persist. To passively compensate for such effects, the use of a common-path optical system holds promise; however, unfortunately, the implementation of a common-path optical system into the JM-DCSP presents challenges due to considerably long time delays in the generation of PCPS. An alternative approach to actively suppress environmental disturbances is to compensate for and stabilize the optical path length variations resulting from environmental disturbances by incorporating another interferometer with a stable CW laser light [17]. Nevertheless, constructing an optical system to control the optical path length of multiple PCPs and reference pulse is challenging.

The placement of samples to acquire interferograms with and without samples is also a factor that can induce environmental disturbances. To address this issue and achieve high-precision measurements, an interesting approach has been reported [18]. In this approach, the sample is fixed on a moving stage, and the interferograms with and without the sample are obtained by moving the sample on the stage. This method enables the acquisition of interferograms without introducing environmental disturbances. By repeating this measurement iteratively and performing signal accumulation, it is believed that fluctuations in the absolute phase caused by environmental disturbances can be suppressed effectively.

5. Conclusions

In this article, we developed JM-DCSP, a technique that combines OFC and DCS with spectroscopic polarimetry to obtain the Jones matrix of a sample's polarization response as a function of wavelength. By multiplexing incident light into two different polarizations and utilizing precise time delays, JM-DCSP enables rapid and polarization-modulation-free acquisition of optical spectra of Jones matrix elements. The effectiveness of JM-DCSP was demonstrated by measuring polarization elements with known properties, such as a quarter-wave plate and a Faraday rotator. The experimental results showed good agreement with theoretical values, validating the proposed method for Jones matrix analysis of optical materials. We discuss the influence of environmental disturbances on the absolute phase measurements and suggested possible approaches for improvement in future implementations. Overall, JM-DCSP offers a promising technique for detailed analysis of the polarization response of samples and has potential applications in various fields, including materials characterization and biological sample investigation.

Acknowledgments

This work was supported by the Japan Society for the Promotion of Science (20J23577, 22H00303), Cabinet Office, Government of Japan (Subsidy for Reg. Univ. and Reg. Ind. Creation), and Research Clusters program of Tokushima University (2201001).

Author declarations

Conflict of Interest

The authors have no conflicts to disclose.

Author Contributions

Hidenori Koresawa: Conceptualization (equal); Data curation (lead); Formal analysis (lead); Investigation (equal); Methodology (equal); Validation (lead); Writing - original draft (equal); Writing - review & editing (equal). **Hiroki Kitahama:** Data curation (supporting); Formal analysis (supporting); Investigation (supporting); Methodology (supporting). **Eiji Hase:** Formal analysis (supporting); Investigation (supporting); Methodology (supporting). **Yu Tokizane:** Formal analysis (supporting); Investigation (supporting); Methodology (supporting). **Akifumi Asahara:** Formal analysis (supporting); Methodology (supporting). **Takeo Minamikawa:** Conceptualization (supporting); Formal analysis (supporting); Investigation (supporting); Methodology (supporting); Supervision (supporting); Validation (supporting). **Kaoru Minoshima:** Formal analysis (supporting); Methodology (supporting). **Takeshi Yasui:** Conceptualization (equal); Funding acquisition (lead); Investigation (supporting); Methodology (supporting); Project administration (lead); Supervision (lead); Writing – original draft (equal); Writing – review & editing (equal).

Data availability

The data that support the findings of this study are available from the corresponding author upon reasonable request.

References

[1] H. Fujiwara, Spectroscopic ellipsometry: principles and applications (Wiley, 2007).

- [2] C. Yim, M. O'Brien, N. McEvoy, S. Winters, I. Mirza, J. G. Lunney, and G. S. Duesberg, "Investigation of the optical properties of MoS₂ thin films using spectroscopic ellipsometry," *Appl. Phys. Lett.* **104**(10), 103114 (2014).
- [3] S. G. Lim, S. Kriventsov, and T. N. Jackson, "Dielectric functions and optical bandgaps of high-K dielectrics for metal-oxide-semiconductor field-effect transistors by far ultraviolet spectroscopic ellipsometry," *J. Appl. Phys.* **91**(7), 4500-4505 (2002).
- [4] K. Spaeth, A. Brecht, and G. Gauglitz, "Studies on the biotin-avidin multilayer adsorption by spectroscopic ellipsometry," *J. Colloid Interface Sci.* **196**(2), 128-135 (1997).
- [5] R. M. A. Azzam, "Photopolarimetric measurement of the Mueller matrix by Fourier analysis of a single detected signal," *Opt. Lett.* **2**(6), 148-150 (1978).
- [6] T. Minamikawa, Y. Hsieh, K. Shibuya, E. Hase, Y. Kaneoka, S. Okubo, H. Inaba, Y. Mizutani, H. Yamamoto, T. Iwata, and T. Yasui, "Dual-comb spectroscopic ellipsometry," *Nat. Commun.* **8**(1), 610 (2017).
- [7] H. Koresawa, M. Gouryeb, K. Shibuya, T. Mizuno, E. Hase, Y. Tokizane, R. Oe, T. Minamikawa, and T. Yasui, "Dynamic characterization of polarization property in liquid-crystal-on-silicon spatial light modulator using dual-comb spectroscopic polarimetry," *Opt. Express* **28**(16), 23584-23593 (2020).
- [8] R. Zhang, L. Shi, S. Zhou, J. Zhang, B. Liu, and G. Wu, "Dynamic ellipsometry measurement based on a simplified phase-stable dual-comb system," *Opt. Express* **30**(5), 7806-7820 (2022).
- [9] K. Hinrichs, B. Blevins, A. Furchner, N. S. Yadavalli, S. Minko, R. Horvath, and M. Mangold, "Mid-infrared dual-comb polarimetry of anisotropic samples," *Nat. Sci.*

3(2), e20220056 (2023).

- [10] Th. Udem, J. Reichert, R. Holzwarth, and T. W. Hänsch, "Accurate measurement of large optical frequency differences with a mode-locked laser," *Opt. Lett.* **24**(13), 881-883 (1999).
- [11] M. Niering, R. Holzwarth, J. Reichert, P. Pokasov, Th. Udem, M. Weitz, T. W. Hänsch, P. Lemonde, G. Santarelli, M. Abgrall, P. Laurent, C. Salomon, and A. Clairon, "Measurement of the hydrogen 1S-2S transition frequency by phase coherent comparison with a microwave cesium fountain clock," *Phys. Rev. Lett.* **84**(24), 5496–5499 (2000).
- [12] Th. Udem, R. Holzwarth, and T. W. Hänsch, "Optical frequency metrology," *Nature* **416**(6877), 233-237 (2002).
- [13] S. Schiller, "Spectrometry with frequency combs," *Opt. Lett.* **27**(9), 766–768 (2002).
- [14] F. Keilmann, C. Gohle, and R. Holzwarth, "Time-domain mid-infrared frequency-comb spectrometer," *Opt. Lett.* **29**(13), 1542–1544 (2004).
- [15] T. Yasui, Y. Kabetani, E. Saneyoshi, S. Yokoyama, and T. Araki, "Terahertz frequency comb by multifrequency-heterodyning photoconductive detection for high-accuracy, high-resolution terahertz spectroscopy," *Appl. Phys. Lett.* **88**(24), 241104 (2006).
- [16] I. Coddington, N. Newbury, and W. Swann, "Dual-comb spectroscopy," *Optica* **3**(4), 414-426 (2016).
- [17] H. Koresawa, E. Hase, Y. Tokizane, T. Minamikawa, and T. Yasui, "Combination of dual-comb spectroscopy with Jones-matrix polarimetry," *Tech. Digest 15th Pacific Rim Conference on Lasers and Electro-Optics 2022*, P-CTh6-09 (2022).

[18] K. A. Sumihara, S. Okubo, M. Okano, H. Inaba, and S. Watanabe, "Ultra-precise determination of thicknesses and refractive indices of optically thick dispersive materials by dual-comb spectroscopy," *Opt. Express* **30**(2), pp. 2734-2747 (2022).